J|A|C|S
COMMUNICATIONS

Published on Web 04/27/2006

Inorganic Single Wall Nanotubes of $SbPS_{4-x}Se_x$ ($0 \leq x \leq 3$) with Tunable Band Gap

Christos D. Malliakas and Mercouri G. Kanatzidis*

Department of Chemistry, Michigan State University, East Lansing, Michigan 48824

Received November 22, 2005; E-mail: kanatzid@cem.msu.edu

Since the discovery of carbon nanotubes,[1] researchers have focused on unraveling their intriguing properties and finding applications. "Inorganic" nanotubes, however, could have at least as many diverse properties and applications as their carbon counterparts. Their availability in bulk prepared via rational synthesis techniques could greatly facilitate the development of this new area of materials science. Inorganic materials have a wide range of useful properties that might be exploited in nanotube and nanowire form, including high-temperature superconductivity for low-loss electrical power delivery, optical nonlinearity, photoluminescence, enormous magnetoresistivity for information storage, and ferroelectric and ferromagnetic properties for quantum computing and spintronics applications.[2,3] Semiconducting hollow nanotubes could be advantageous in nanoscale electronics, optoelectronics, and biochemical sensing applications.[4] Generally, however, it is a synthetic challenge to produce high quality and quantity inorganic nanotubes. In most cases, special nonequilibrium conditions of synthesis are used to force materials that do not normally form nanotubes to do so. Such methods, which include chemical vapor deposition, flash and discharge evaporation, often give mixtures of various shapes and sizes.[5] Several purification steps may be needed to obtain nanotubes of the same size, resulting in low yields and added cost. To date, examples of inorganic nanotube materials include MS_2 (M = Mo,[6] W,[7] Ta[8]), BN,[9] $NbSe_2$,[10] V_2O_5,[11] magnetite (Fe_3O_4),[12] and $LiMo_3Se_3$[13] with remarkable physical and chemical properties.

Here we describe an inorganic semiconducting system which spontaneously grows as single wall nanotubes in ~95% yield (PXRD). We report the preparation of high quality crystalline $SbPS_{4-x}Se_x$ ($0 \leq x \leq 3$), which adopts an infinite nanotube structure of ~1.3 nm diameter.[14] We determined the crystal structure of the little known $SbPS_4$ system[15] using single-crystal X-ray diffraction and high-resolution transmission electron microscopy (HRTEM). We also report the isostructural $SbPS_{4-x}Se_x$ ($1 \leq x \leq 3$) analogues.

The structure of $SbPS_4$ consists of a unique tubular arrangement of Sb^{3+} ions and $[PS_4]^{3-}$ tetrahedra (Figure 1A).[16] Pairs of $SbPS_4$ units which are connected through Sb−S bonds are arranged in isosceles triangles. These triangular units are stacked with a 60° rotation and linked through Sb−S−P bonds to form a hollow tubular structure (Figure 1B). Three S atoms of each $[PS_4]^{3-}$ unit bind to three formally Sb^{3+} ions, each of which belongs to adjacent isosceles triangles. The fourth terminal S atom and the putative lone pair of electrons of all Sb^{3+} ions point toward the interior of the tube.

$SbPS_4$ naturally crystallizes in a unique nanotube form. The van der Waals gap between the $SbPS_4$ nanotubes is around 1.6 Å. The external diameter of the tube is around 13 Å, and the trigonal antiprism-shaped cavity formed by the internal sulfur atoms has a diameter of around 2.3 Å and a height of 3 Å (excluding van der Waals radii). Both the interior and the exterior surfaces of the nanotubes are lined with sulfur atoms. The weak inter-tube van der Waals (vdW) interactions are responsible for considerable sliding of the tubes passed one another. This results in loss of crystallographic registry and in fiber-like diffraction properties, which makes it extremely difficult to find suitable single-crystal samples for structure determination. The overall packing of the tubes, however, remains close hexagonal. Functionalized S-rich surfaces of this type and vdW gaps can be reactive toward heavy metals, and such materials can be used as environmental remediation agents.[17]

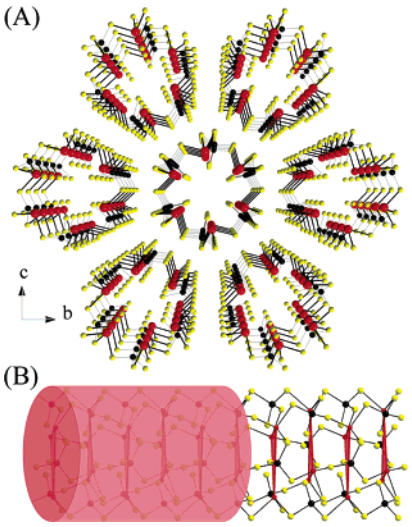

Figure 1. (A) Structure of $SbPS_4$ nanotubes perspective viewed along the direction of the crystal growth of the tube (*a*-axis). (B) Structure of one isolated nanotube. The arrangement and stacking of antimony atoms along the *a*-axis is shown with red triangles. Yellow atoms are S, black P, and red Sb atoms. The Sb−S bond distance range is 2.49(1)−2.62(1) Å. The $P-S_b$ and $P-S_t$ are 2.07(1) and 2.00(1) Å, respectively (S_b and S_t are bridging and terminal S atoms).

The fibrous nature of $SbPS_4$ is obvious by visual inspection. Scanning Electron Microscopy (SEM) shows the formation of bundles of $SbPS_4$ nanotubes with different diameters in the range of 0.2−20 μm. The length of the fibers reaches centimeter length scales. HRTEM[18] verified the presence of individual nanotubes and the formation of bundles due to van der Waals interactions (Figure 2A). The diameter of an individual nanotube is ~1.4 nm, as measured from the TEM image, which is very close to the value of 1.3 nm found by the crystallographic model. The selected area electron diffraction pattern of Figure 2A (inset) verified the single crystalline organization of the nanotubes and their growth direction along the short *a*-axis.

The $SbPS_4$ nanotubes are orange−yellow with an optical band gap at 2.57 eV. They are transparent in the mid-infrared region down to ~600 cm^{-1}. The material is insoluble in common polar solvents at room temperature, such as water, *N*,*N*-dimethylformamide, *N*-methylformamide, and ethylenediamine, and nonpolar solvents, such as carbon disulfide, benzene, and hexane. Remark-

10.1021/ja057943m CCC: $33.50

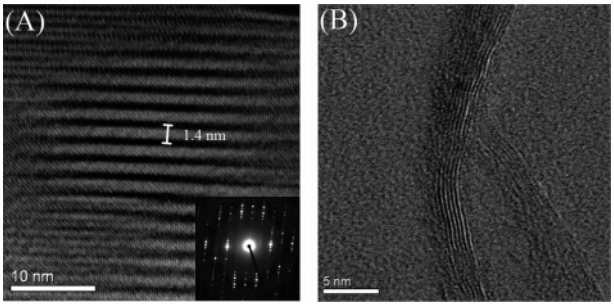

Figure 2. (A) TEM image of a $SbPS_4$ bundle. The uniform diameter and alignment of the individual nanotubes are apparent. Selected area electron diffraction pattern (inset) indicates single crystalline character on the nanoscale. (B) HRTEM image of individual nanofiber bundles of $SbPS_4$ after dispersion by sonication in DMF. Additional images are given in the Supporting Information.

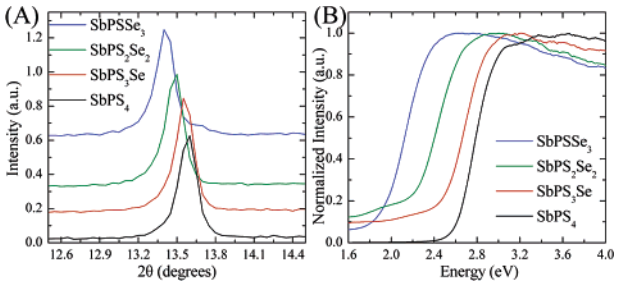

Figure 3. (A) Shift of the (020) reflection in the powder X-ray pattern of the $SbPS_{4-x}Se_x$ analogues as a result of the sulfur substitution in the $[PS_4]^{3-}$ unit. (For cell parameters, see Supporting Information, Table 1S.) (B) Optical band gap measurement of the $SbPS_{4-x}Se_x$ series (ground samples). The gap decreases as the amount of Se increases.

ably, the material is insoluble even in concentrated hydrochloric acid, which can easily dissolve possible Sb_2S_3 impurities. Mass spectrometry (MS) on the acid-treated $SbPS_4$ shows evaporation of absorbed HCl molecules at ~120 °C ($<10^{-5}$ Torr), indicating small molecule accessibility of the cavities in the nanotubes (see Supporting Information, Figure 3S). The material can be dispersed, however, with sonication in polar solvents, such as DMF, NMF, and acetonitrile, to form nanoaggregates of bundles of $SbPS_4$. This can be seen experimentally by TEM (Figure 2B).

Interestingly, up to three S atoms can be substituted with Se atoms in the $[PS_4]^{3-}$ tetrahedron to give the isostructural phases $SbPS_{4-x}Se_x$ ($1 \leq x \leq 3$).[19] The gradual substitution of the S atom with the larger and heavier Se atom affects the size and diameter of the nanotubes uniformly. The expansion of the cell is shown in Figure 3A from the shift of the position of the (020) reflection. The diameter distribution of the nanotubes in every $SbPS_{4-x}Se_x$ ($0 \leq x \leq 3$) analogue is extremely narrow since no broadening or multiple phases are present in the powder pattern. As a result of the difference in the diameter of the $SbPS_{4-x}Se_x$ nanotubes and the S substitution, the electronic properties also change accordingly. The band gap (E_g) decreases from 2.57 eV for $SbPS_4$ to 1.90 eV as the amount of Se increases in the $SbPS_{4-x}Se_x$ series. Specifically, for $SbPS_3Se$, E_g drops to 2.42 eV, for $SbPS_2Se_2$ to 2.13 eV, and for $SbPSSe_3$ to 1.90 eV (Figure 3B). Electronic band calculations at the density functional theory (DFT) level suggest a direct band gap in $SbPS_4$ with the top of the valence band based predominantly on S p-orbitals and the bottom of the conduction band based on Sb p-orbitals (see Supporting Information, Figure 11S). This is consistent with the observed narrowing of the energy gap with Se substitution.

A simple reaction of the elements under thermodynamically controlled equilibrium conditions suffices to produce high yield of bundles of inorganic semiconducting $SbPS_{4-x}Se_x$ nanotubes. In fact, this is a rare example of well enough crystallized nanotubes to be able to determine their atomic structure. Manipulation of the band gap was achieved by gradual substitution of sulfur atoms in the $[PS_4]^{3-}$ unit by selenium atoms. The nanometer scale diameter of the $SbPS_{4-x}Se_x$ nanotubes and their inner tunnel space may be used for guest−host chemistry for small molecules or atoms (<2.3 Å in size). Further work to explore the optical and absorption properties of these materials is currently underway.

Acknowledgment. We thank the National Science Foundation for support (DMR-0443785). SEM, EDS, and TEM studies were conducted at the Center for Advanced Microscopy at MSU. We thank D. Bilc and Professor S. D. Mahanti for the band calculations, and Rui Huang for the MS measurements.

Supporting Information Available: Details of structural analysis in CIF format, X-ray powder patterns, MS, IR plots, SEM, TEM images, and band calculations. This material is available free of charge via the Internet at http://pubs.acs.org.

References

(1) Iijima, S. *Nature* **1991**, *354*, 56.
(2) Law, M.; Sirbuly, J. D.; Johnson, C. J.; Goldberger, J.; Saykally, J. R.; Yang, P. *Science* **2004**, *305*, 1269.
(3) Nath, M.; Kar, S.; Raychaudhuri, A. K.; Rao, C. N. R. *Chem. Phys. Lett.* **2003**, *368*, 690.
(4) Goldberger, J.; He, R.; Zhang, Y.; Lee, S.; Yan, H.; Choi, H.; Yang, P. *Nature* **2003**, *422*, 599.
(5) Remskar, M. *Adv. Mater.* **2004**, *16*, 1497.
(6) Feldman, Y.; Wasserman, E.; Srolovitz, D. J.; Tenne, R. *Science* **1995**, *267*, 222.
(7) Tenne, R.; Margulis, L.; Genut, M.; Hodes, G. *Nature* **1992**, *360*, 444.
(8) Nath, M.; Rao, C. N. R. *J. Am. Chem. Soc.* **2001**, *123*, 4841.
(9) Chopra, N. G.; Luyken, R. G.; Cherrey, K.; Crespi, V. H.; Cohen, M. L.; Louie, S. G.; Zettl, A. *Science* **1995**, *269*, 966.
(10) Galvan, D. H.; Kim, J. H.; Maple, M. B.; Avalos-Berja, M.; Adem, E. *Fullerene Sci. Technol.* **2000**, *8*, 143.
(11) Satshkumar, B. C.; Govindaraj, A.; Vogl, M. E.; Basumallick, L.; Rao, C. N. R. *J. Mater. Res.* **1997**, *12*, 604.
(12) Liu, Z.; Zhang, D.; Han, S.; Li, C.; Lei, B.; Lu, W.; Fang, J.; Zhou, C. *J. Am. Chem. Soc.* **2005**, *127*, 6.
(13) Tarascon, J. M.; Hull, G. W.; DiSalvo, F. J. *Mater. Res. Bull.* **1984**, *19*, 915.
(14) Stoichiometric amounts of the elements (3.3 mmol Sb, 3.3 mmol P, and 13.2 mmol S for $SbPS_4^-$ and corresponding amounts for $SbPS_3Se$, $SbPS_2Se_2$, and $SbPSSe_3$) were loaded into fused silica tubes and sealed under vacuum ($<10^{-4}$ Torr). The mixture temperature was increased to 200 °C over 6 h, kept there for 4 h, then increased to 650 °C over 12 h and kept there for 2 days before being cooled to 50 °C at 12 °C/min. Electron microprobe energy dispersive spectroscopy (EDS) was performed on several crystals and confirmed the presence and expected relative ratio of the elements to within ±4%. EDS analyses were performed on a JEOL JSM-35C scanning electron microscope with a Noran Vantage EDS detector.
(15) (a) D'ordyai, V. S.; Galagovets, I. V.; Peresh, E. Yu.; Voroshilov, Yu. V.; Gerasimenko, V. S.; Slivka, V. Yu. *Zh. Neorg. Khim.* **1979**, *24*, 2886. (b) Andrae, H.; Blachnik, R. *J. Alloys Compd.* **1992**, *189*, 209.
(16) A STOE IPDS II diffractometer was used to collect intensity data with graphite monochromatized Mo Kα (λ = 0.71073 Å) radiation. An analytical absorption correction was applied using the program X-RED (routine within the X-AREA software package). The structure of the $SbPS_4$ single crystal was refined with SHELXL software (Sheldrick, G. M. *SHELXL*; University of Göttingen, 2002). A stable refinement was accomplished only in the triclinic space group *P*1. Single-crystal X-ray diffraction data for $SbPS_4$: triclinic cell, space group *P*1, a = 6.2719(14) Å, b = 13.059(4) Å, c = 22.493(6) Å, α = 90.09(2)°, β = 90.065(19)°, γ = 91.76(2)°, V = 1841.4(8) Å^3, Z = 12, ρ_{calc} = 3.040 g/cm^3, T = 298(2) K, λ = 0.71073 Å, 2θ = 40.00°. Refinement of 326 parameters on 3287 independent reflections out of 6385 measured reflections (R_{int} = 0.0946) led to R_1 = 0.1170 ($I > 2\sigma(I)$), wR_2 = 0.2657 (all data), and S = 1.222 with the largest difference peak and hole of 8.403 and −1.747 e$^-$/Å^3. Cavity size was measured with the CAVITY routine within the PLATON software package.
(17) Feng, X.; Fryxell, G. E.; Wang, L.-Q.; Kim, A. Y.; Liu, J.; Kemner, K. M. *Science* **1997**, *276*, 924.
(18) A small amount of $SbPS_4$ fibers was sonicated in DMF for a few minutes as an attempt to separate the nanotubes.
(19) Phase purity was evaluated with powder X-ray diffraction with a Rigaku rotating Cu anode diffractometer. The $SbPS_{4-x}Se_x$ were identified by comparing the experimental patterns to ones calculated from the $SbPS_4$ single-crystal structure. $Sb_2S_xSe_{3-x}$ impurities were also identified in the powder patterns. For x = 4 ($SbPSe_4$), the reaction gives Sb_2Se_3 and P_ySe_z.

JA057943M